Journal of Translational Medicine

RESEARCH

Open Access

BRCC36 regulates β-catenin ubiquitination to alleviate vascular calcification in chronic kidney disease

Yalan Li[1†], Xiaoyue Chen[1†], Yiqing Xiong[1†], Xueqiang Xu[1], Caidie Xie[3], Min Min[1], Dongmei Liang[1], Cheng Chen[2*] and Huijuan Mao[1*]

Abstract

Background The prevalence of vascular calcification (VC) in chronic kidney disease (CKD) patients remains substantial, but currently, there are no effective pharmaceutical therapies available. BRCA1/BRCA2-containing complex subunit 36 (BRCC36) has been implicated in osteoblast osteogenic conversion; however, its specific role in VC remains to be fully elucidated. The aim of this study was to investigate the role and underlying mechanisms of BRCC36 in VC.

Methods The association between BRCC36 expression and VC was examined in radial arteries from patients with CKD, high-adenine-induced CKD mice, and vascular smooth muscle cells (VSMCs). Western blotting, real-time polymerase chain reaction, immunofluorescence, and immunohistochemistry were used to analyse gene expression. Gain- and loss-of-function experiments were performed to comprehensively investigate the effects of BRCC36 on VC. Coimmunoprecipitation and TOPFlash luciferase assays were utilized to further investigate the regulatory effects of BRCC36 on the Wnt/β-catenin pathway.

Results BRCC36 expression was downregulated in human calcified radial arteries, calcified aortas from CKD mice, and calcified VSMCs. VSMC-specific BRCC36 overexpression alleviated calcium deposition in the vasculature, whereas BRCC36 depletion aggravated VC progression. Furthermore, BRCC36 inhibited the osteogenic differentiation of VSMCs in vitro. Rescue experiments revealed that BRCC36 exerts the protective effects on VC partly by regulating the Wnt/β-catenin signalling pathway. Mechanistically, BRCC36 inhibited the Wnt/β-catenin pathway by decreasing the K63-linked ubiquitination of β-catenin. Additionally, pioglitazone attenuated VC partly through upregulating BRCC36 expression.

Conclusions Our research results emphasize the critical role of the BRCC36-β-catenin axis in VC, suggesting that BRCC36 or β-catenin may be promising therapeutic targets to prevent the progression of VC in CKD patients.

Keywords Chronic kidney disease, Vascular calcification, Ubiquitin–proteasome degradation, BRCC36, β-catenin

[†]Yalan Li, Xiaoyue Chen, and Yiqing Xiong are contributed equally to this work.

*Correspondence:
Cheng Chen
yishixingtaicc@163.com
Huijuan Mao
maohuijuan72@njmu.edu.cn
Full list of author information is available at the end of the article

Graphical Abstract

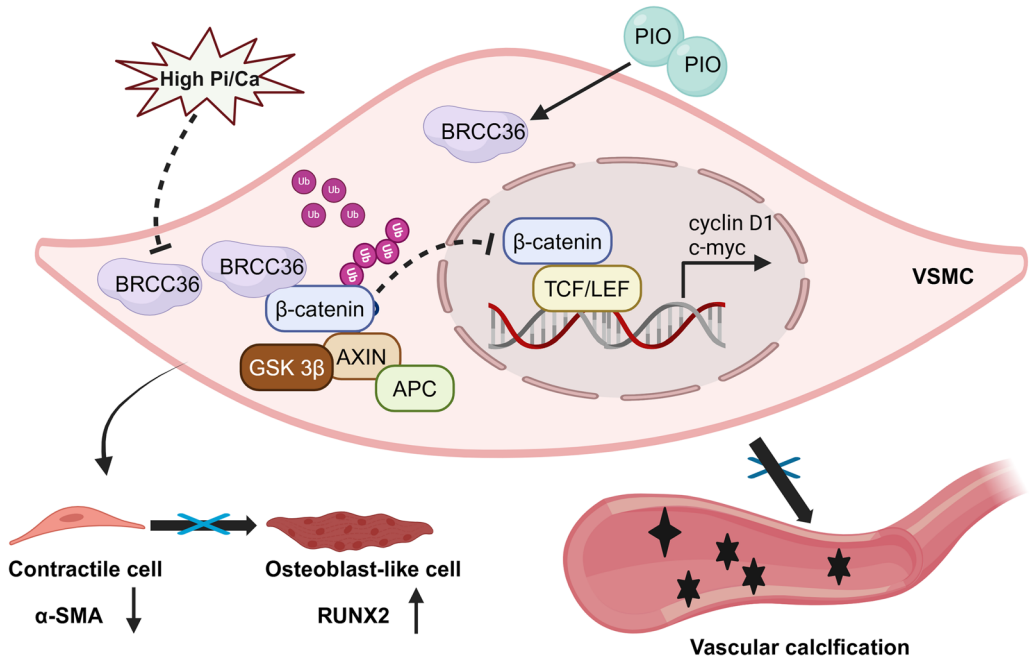

Introduction

The incidence of vascular calcification (VC) in patients with chronic kidney disease (CKD) is extremely high, and its severity is closely related to the risk of cardiovascular disease (CVD) mortality and all-cause mortality [1]. Given that VC is an independent risk factor for adverse cardiovascular events in CKD patients, the imperative to develop effective pharmacological interventions to prevent VC progression underscores the importance of elucidating the pathogenesis of VC [2]. Currently, VC is recognized as an active cell-mediated process similar to osteogenesis, characterized by the ectopic deposition of hydroxyapatite [3]. The pathogenesis mainly encompasses inflammatory states, abnormalities in calcium-phosphate metabolism, the osteogenic differentiation of vascular smooth muscle cells (VSMCs), and epigenetic dysregulation [4–7]. Impeding the osteogenic differentiation of VSMCs is a key scientific issue and a hot topic of current research.

The Wnt/β-catenin signalling pathway plays a critical role in VC [8]. In our previous study, we reported Wnt/β-catenin overactivation and enhanced β-catenin nuclear cotranslocation during VC progression [9]. β-catenin (CTNNB1) is a major mediator of the canonical Wnt/β-catenin signalling pathway and is composed of a central region with 12 armadillo repeats, an amino (N) terminus, and a carboxyl (C) terminus domain [10]. Although numerous studies have indicated that β-catenin can be regulated by multiple posttranslational modifications, including phosphorylation, ubiquitination, acetylation, and S-nitrosylation, the importance of the biological functions of β-catenin regulated by ubiquitination is becoming widely appreciated [11–14]. The core event in the Wnt/β-catenin signalling pathway involves the nuclear translocation and stabilization of β-catenin, a process that is finely regulated by ubiquitination [15, 16]. There is a consensus that the activation of Wnt/β-catenin signalling contributes to VC; however, there have been no successful clinical trials of developed β-catenin-targeted drugs. Targeting the ubiquitin–proteasome system (UPS) with clinical translational potential holds much promise for therapeutic development and clinical applications.

BRCA1/BRCA2-containing complex subunit 36 (BRCC36), a deubiquitinating enzyme discovered in 2003, belongs to the JAMM/MPN family and is encoded by the BRCC36 gene [17]. BRCC36 regulates various physiological processes, including DNA damage repair, cell autophagy, nucleotide-binding oligomerization domain-like receptor family pyrin domain-containing 3 (NLRP3) inflammasome activation, and signal transduction

[18–21]. Cai et al. suggested a close relationship between BRCC36 and β-catenin in osteoblasts [22]. Recent studies by our research group have demonstrated that BRCC36 can inhibit the osteogenic differentiation of VSMCs by affecting the phosphorylation level of β-catenin in vitro [23]. BRCC36 is also known to modify the activity of its target proteins via lysine (K) 63-dependent deubiquitination [24]. However, how BRCC36 influences arterial medial calcification in CKD mice and whether BRCC36 affects the ubiquitination level of β-catenin in VC are currently unknown.

This study serves as an in-depth supplement to our previous research [23]. We aimed to elucidate the possible role and underlying molecular mechanisms of BRCC36 in VC and revealed that BRCC36 attenuated VC in CKD mice and inhibited the osteogenic differentiation of VSMCs in calcifying medium (CM). Moreover, our mechanistic studies revealed that BRCC36 interacted with and deubiquitinated β-catenin and inhibited Wnt/β-catenin signalling activity. Therefore, targeting BRCC36 or β-catenin appears to be an attractive therapeutic approach to slow VC progression.

Materials and methods

Human samples

Human radial artery samples were collected from CKD patients undergoing arterial venous fistula operations. All procedures were conducted in accordance with the Declaration of Helsinki and approved by the Human Research Ethics Committee of the First Affiliated Hospital of Nanjing Medical University (approval number: 2024-SR-251). Informed consent was obtained from all participants before sample collection.

Murine models of CKD

The animal experiments in this study were approved by the Institutional Animal Ethics Committee of Nanjing Medical University (approval number: IACUC-2312015), and all animal procedures complied with the Guide for National Institutes of Health guidelines. Male C57BL/6J mice aged 8 weeks (body weight = 23–26 g) were purchased from Nanjing Medical University and randomly divided and housed in a special pathogen-free (SPF) environment at constant temperature and humidity with a 12-h light–dark cycle. VSMC-specific BRCC36-overexpressing mice (AAV-BRCC36 OE) and VSMC-specific BRCC36-knockout mice (AAV-shBRCC36) were generated via tail vein injection of a recombinant adeno-associated virus driven by the smooth muscle protein 22-alpha (SM22α) promoter (Hanbio Biotechnology Co., Ltd., China). The CKD mouse VC model was established by feeding mice a special chow containing high levels of adenine (0.2%) and phosphate (1.2%). Six percent casein was added to the adenine diet to cover the taste and smell of adenine. The control group was fed a standard pellet chow diet (normal diet). After 12 weeks, all mice were anaesthetized and euthanized, and their serum and aortas were collected for further analysis.

Cell culture and transfection

Primary vascular smooth muscle cells (VSMCs) were extracted from 8-week-old C57BL/6J mice using the tissue explant method. Briefly, the mice were euthanized via intraperitoneal sodium pentobarbital, and the aorta was isolated. After the intima and adventitia were removed, the aorta was finely chopped into 1 mm^2 pieces and cultured in complete medium (DMEM/F12, Gibco, USA, A4192002) supplemented with 10% fetal bovine serum (FBS, Sciencell, USA, 0500), 100 U/ml penicillin and 100 mg/ml streptomycin (KeyGEN, China, KGL2303-100), at 37 °C in 5% CO_2. VSMCs at passages 3 to 8 were used for the experiments. To induce calcification, VSMCs were maintained in calcifying medium (CM) comprising DMEM/F12 supplemented with 10% FBS, 10 mmol/L of β-glycerophosphate, 50 μg/mL ascorbic acid, and 0.1 μmol/L of dexamethasone for 7 days, with the medium changed every 2 days.

Adenovirus-mediated BRCC36 overexpression and small interfering RNA (siRNA)-induced BRCC36 depletion were used to investigate the function of BRCC36 in VC. VSMCs were evenly seeded into 6-well plates and incubated with adenovirus for 48 h to induce BRCC36 overexpression. siRNAs targeting BRCC36 were designed and synthesized by Nanjing Zebrafish Biotech Co.,Ltd. The relevant siRNAs are listed in Supplementary Table 1. Briefly, VSMCs were seeded into 6-well plates one day before transfection and were then transfected with siRNAs using Lipofectamine 8000 (Beyotime, China, C0533) according to the manufacturer's instructions.

Western blot

Proteins were extracted from mouse aortic tissues or VSMCs using precooled radioimmunoprecipitation (RIPA) lysis buffer (FDbio, China, fd009) containing protease and phosphatase inhibitors (FDbio, China, fd1001). The samples were then centrifuged at 12,000 rpm for 10 min at 4 °C. A bicinchoninic acid (BCA) protein assay kit (KeyGEN, China, KGB2101-1000) was used to quantify the protein concentrations in the lysates. Equal amounts of protein were loaded onto sodium dodecyl polyacrylamide gels with different polyacrylamide

concentrations, electrophoresed, and transferred to polyvinylidene fluoride membranes (PVDF, Millipore, USA, 03,010,040,001). After being blocked in 5% nonfat dry milk (Beyotime, China, P0216) for at least 1 h, the membranes were incubated with specific primary antibodies at 4 °C overnight. The primary antibodies used in the research are listed in Supplementary Table 2. The following day, the membranes were washed with Tris-buffered saline with 0.1% Tween-20 (TBST) at least three times and incubated with the corresponding secondary antibody (FDbio, China, fd007) at room temperature for 1 h. Bands were visualized by enhanced chemiluminescence (ECL, FDbio, China, fd8020), and images were captured with a ChemiDoc MP (BioRad, China). The western blot bands were further analysed via ImageJ (NIH, USA).

RNA extraction, reverse transcription, and quantitative real-time PCR

Total RNA from VSMCs was extracted using an RNA isolation kit (Vazyme, China, RC112-01). The RNA was reverse transcribed into cDNA using the HiScript III RT SuperMix (Vazyme, China, R323-01). Quantitative reverse transcription–polymerase chain reaction (PCR) was conducted using SYBR qPCR Master Mix (Vazyme, China, Q711-02) on a real-time PCR system (Roche, Switzerland) according to the manufacturer's instructions. The relative gene expression data were normalized to that of GAPDH and calculated using the 2-ΔΔCT method. The primer sequences are shown in Supplementary Table 3.

Immunohistochemistry (IHC) staining

Mouse aortic tissue was isolated, fixed in 4% paraformaldehyde (PFA) overnight, embedded in paraffin, and sectioned continuously at a thickness of 4 mm. After routine dewaxing and antigen retrieval, the deparaffinized sections were washed with phosphate buffered solutions (PBS, Biosharp, China, BL601A) three times. The sections were blocked with 10% goat serum (Solarbio Science & Technology, China, SL038) to block nonspecific antigens and were then incubated with primary antibodies (diluted according to manufacturers' recommendations) at 4 °C overnight. The next day, the sections were incubated with HRP-conjugated secondary antibodies (MXB, China, KIT-5920) for 1 h at room temperature. After being washed with PBS, the sections were stained with diaminobenzidine (DAB) working solution, and counterstained with haematoxylin (KeyGEN, China, KGE1201-100) to visualize nuclei. Finally, images were acquired under an optical microscope (Olympus, Japan).

Immunofluorescence (IF) staining

After sections were dewaxed or VSMCs were fixed with 4% PFA, the samples were permeabilized with 0.3% Triton X-100 in PBS for 20 min. After being blocked with 10% goat serum (Solarbio Science & Technology, China, SL038), the samples were washed three times with PBS and then incubated with primary antibodies overnight at 4 °C. After rewarming for 15 min, the tissue sections and cells were stained with fluorescently labelled secondary antibodies (Abways, China, AB0151). The nuclei were counterstained with 4',6- diamidino-2-phenylindole (DAPI, Beyotime, China, P0131). Images were captured using a THUNDER DMi8 microscope (Germany).

Alizarin Red S staining and Von Kossa staining

For Alizarin Red S staining, artery tissue sections were dewaxed and stained with 2% Alizarin Red S solution (pH 4.2, Solarbio Science & Technology, China, G1452) for 20 min at room temperature. After a quick rinse in distilled water, the positively stained areas appeared orange–red. The stained sections were dehydrated with graded ethanol and sealed with neutral gum. For en face Alizarin Red S staining of the whole aorta, mouse aortic tissue was fixed in 95% ethanol for one day and stained with 0.003% Alizarin Red S in 1% potassium for another day; calcified areas were coloured red. After treatment, VSMCs were washed with PBS for three times and fixed in 4% PFA for 20 min. The fixed cells were then stained with 2% Alizarin Red S solution for 20 min at room

(See figure on next page.)

Fig. 1 BRCC36 levels are decreased during vascular calcification. **A** Representative Masson staining, Alizarin Red S staining, chest CT, IHC staining of RUNX2 and BRCC36 antibody in CKD patients without and with VC. Scale bar, 50 μm. n = 5 per group. **B** Representative IF staining of BRCC36 (red), α-SMA (green), and DAPI (blue) in CKD patients without and with VC. Scale bar, 100 μm. n = 5 per group. **C** Representative Masson staining in control and CKD kidneys. **D** Serum creatinine (Cr), serum blood urea nitrogen (BUN), serum phosphorus (Pi), and serum calcium (Ca) levels. n = 6 per group. **E** Representative Von Kossa staining and IHC staining of BRCC36 antibody in control and CKD vessels. Scale bar, left two columns: 200 μm; right columns: 50 μm. n = 6 per group. **F** Protein expression of BRCC36 in calcified vessels of CKD mice was measured by western blotting. n = 6 per group. **G** Representative Alizarin Red S staining images in control and calcified VSMCs. **H** RT-PCR analysis of BRCC36 mRNA expression in control and calcified VSMCs. n = 3 per group. **I** Representative IF images and quantitative analysis of BRCC36 expression in control and calcified VSMCs. **J** Protein level and quantitative analysis of BRCC36 in control and calcified VSMCs. n = 3 per group. Statistical significance was assessed using t-test. All values are presented as mean ± SD. $^{*}P < 0.05$

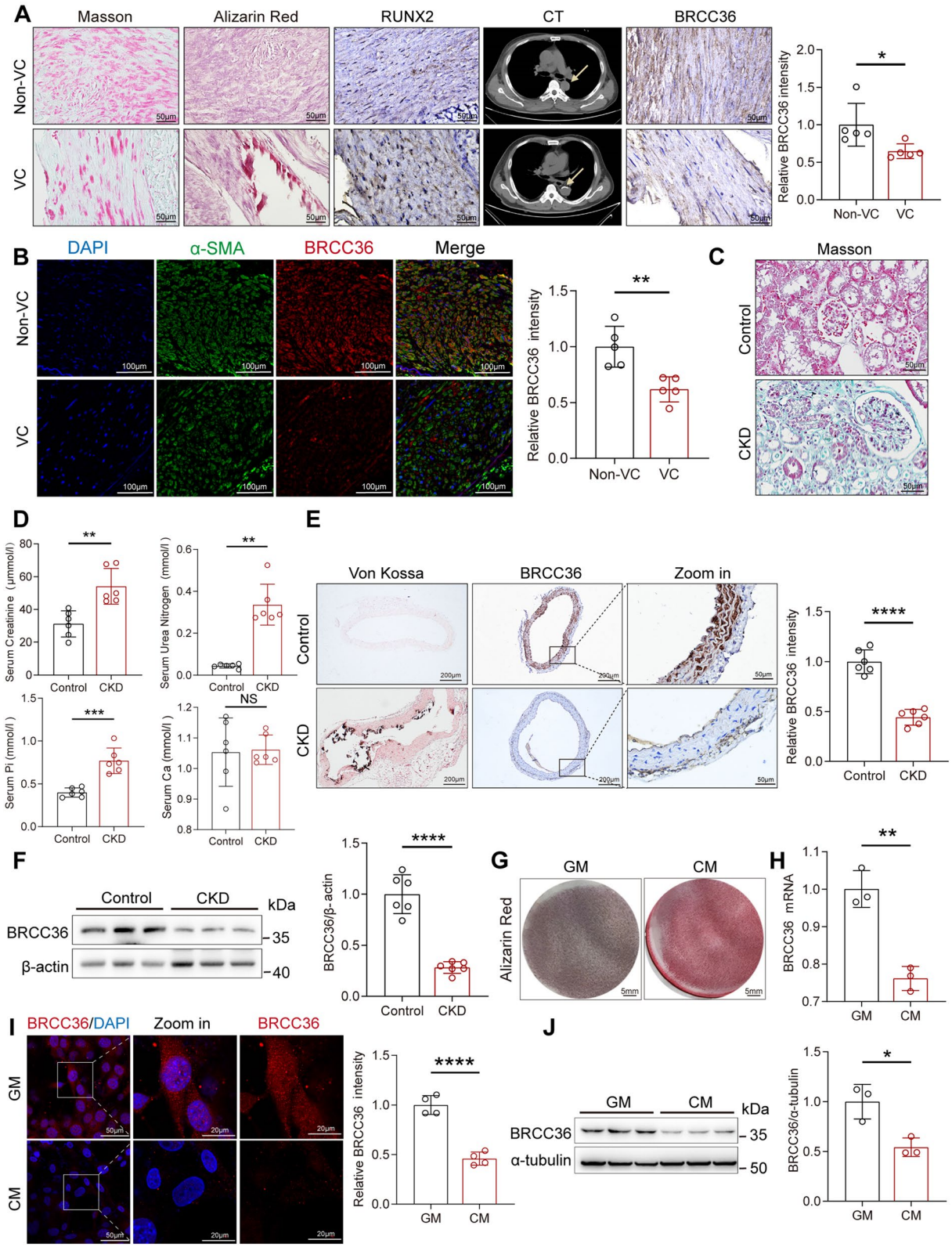

Fig. 1 (See legend on previous page.)

temperature in the dark. Images were captured, followed by quick wash with distilled water. Positively stained cells appeared orange–red.

For Von Kossa staining, deparaffinized artery tissue sections or fixed cells were incubated with 5% silver nitrate (Solarbio Science & Technology, China, G3282) for 2 h under ultraviolet light, and then washed with distilled water. After being treated with 5% sodium sulfate for 5 min, the sections were restained with neutral red for another 5 min. The positively stained area appeared brown or black, and images were acquired under a Nikon ECLIPSE Ti-e inverted microscope (Japan).

TOP/FOPFlash assay

The effect of BRCC36 on the transcriptional activity of β-catenin was assessed using the TOP/FOPFlash assay. VSMCs were seeded into 6-well plates and were transiently transfected with control adenovirus or BRCC36-adenovirus, the TOPFlash reporter gene (Beyotime, China, D2501) or the FOPFlash reporter gene (Beyotime, China, D2503), and Renilla-Luc as an internal control (GeneCopoeia, USA). Forty-eight hours posttransfection, VSMCs were harvested and assayed using a dual luciferase assay system kit (GeneCopoeia, USA, LF004) according to the manufacturer's protocol. Firefly luciferase expression levels were normalized against Renilla luciferase activity.

Coimmunoprecipitation (Co-IP) assays

Protein–protein complexes were obtained from VSMCs and human embryonic kidney 293 T (HEK293T) cells. When the cells reached 80%-90% confluency, they were washed with PBS and then lysed with an appropriate amount of prechilled IP lysis buffer (Absin, China, abs955). The supernatant was added to Sepharose beads linked to negative control IgG antibody or IP antibody following the manufacturer's instructions. The bead-antibody-antigen complex was rotated overnight at 4 °C at 20 rpm. After centrifugation for 1 min at 12,000 rpm at 4 °C to remove the supernatant, the bead complexes were resuspended in 500 μl of wash buffer; this wash process was repeated two more times. After the final wash, the bead complexes were resuspended in 1 × SDS loading buffer (Beyotime, China, P0015A) and then heated at 95 °C for 2–5 min. The collected samples were subjected to western blot analysis.

Statistical analysis

Statistical analyses were carried out using GraphPad Prism version 9.0 (GraphPad Software, USA). All experiments were repeated with at least three independent biological replicates. The data are presented as means ± standard deviations (SDs). The normality of the data was checked via the Shapiro–Wilk normality test. Statistical significance between two groups was assessed using unpaired two-tailed Student's t tests or the Mann–Whitney U test. Differences among more than two groups were compared using one-way ANOVA. $P < 0.05$ was considered statistically significant.

Results

BRCC36 levels are decreased during vascular calcification

To investigate whether BRCC36 is involved in VC, we first collected radial arteries from uraemic patients undergoing arteriovenous fistula surgery. The degree of calcium deposition was confirmed through Alizarin Red S staining, runt-related transcription factor 2 (RUNX2) IHC staining, and chest CT imaging of patients (Fig. 1A). Compared with those in radial arteries without VC, increases in the collagen content in calcified tissues were detected via Masson's trichrome staining (Fig. 1A). Moreover, the IHC results indicated that BRCC36 levels were significantly lower in calcified vascular tissues than in noncalcified tissues (Fig. 1A). The results were subsequently validated by IF staining of BRCC36 and alpha-smooth muscle actin (α-SMA), which is a contractile phenotype of VSMCs (Fig. 1B).

We then established a CKD mouse model of VC using adenine combined with a high-phosphate diet. The Masson staining, PAS staining, H&E staining, Von Kossa staining, and western blot results demonstrated increased renal fibrosis and significant calcium salt

(See figure on next page.)

Fig. 2 BRCC36 overexpression alleviates vascular calcification in mice. **A** The transfection efficiency of BRCC36 overexpression was verified by western blotting. n = 6 per group. **B** RUNX2, α-SMA and GAPDH immunoblotting in the vessel lysates of control and CKD of AAV-NC and AAV-BRCC36 OE mice, n = 6 per group. **C** Representative Von Kossa staining, Alizarin Red S staining, and IHC staining of RUNX2 images in aortas among all groups. Scale bar, 200 μm. n = 6 per group. **D** Representative IF images of RUNX2 and α-SMA in aortas among all groups. Scale bar, 100 μm. **E** RUNX2, α-SMA and GAPDH immunoblotting in the vessels lysates of control and CKD of AAV-NC and AAV-shBRCC36 mice, n = 6 per group. **F** Representative Von Kossa staining, Alizarin Red S staining, and IHC staining of RUNX2 antibody images in aortas among all groups. Scale bar, 200 μm. n = 6 per group. **G** Statistical analysis of RUNX2 was performed. **H** Representative IF images of RUNX2 and α-SMA in aortas among all groups. Scale bar, 100 μm. **I** Representative Alizarin Red S staining images of the whole aortas. Scale bar, 5 mm. Statistical significance was assessed using two tailed t-test (**A**) and 1-way ANOVA followed by Dunnett's test (**B**, **C**, **E**, **G**). All values are presented as mean ± SD. **P* < 0.05

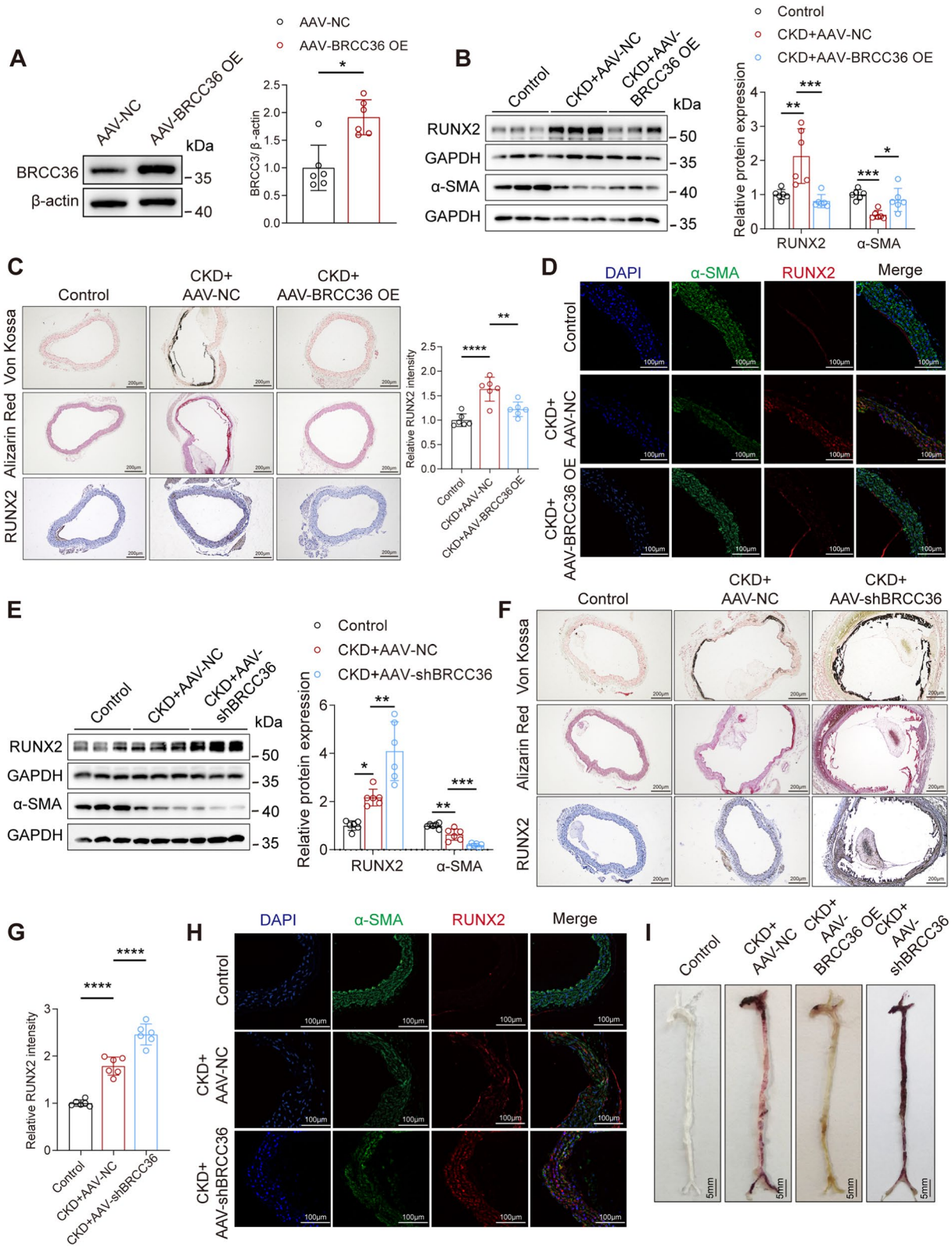

Fig. 2 (See legend on previous page.)

deposition in the model group (Fig. 1C and Fig. S1A, B). The serum creatinine (Cr), blood urea nitrogen (BUN), and phosphate (Pi) levels were significantly elevated in the model group, confirming the successful establishment of the CKD mouse model (Fig. 1D). Von Kossa staining revealed prominent black calcium salt deposits in the vascular media and significant damage to the arterial structure in the model group. The decrease in BRCC36 expression was confirmed by IHC staining and western blotting (Fig. 1E, F).

Additionally, to determine whether BRCC36 participates in the osteogenic differentiation of VSMCs, primary VSMCs were isolated and cultured (see Fig. S1C for cell phenotyping) in CM. Alizarin Red S staining confirmed that CM successfully induced VSMC calcification (Fig. 1G). Over the course of osteogenic induction, the mRNA and protein levels of BRCC36 were significantly lower in calcified VSMCs than in control VSMCs (cultured in growth medium (GM)) (Fig. 1H, J). IF experiments also confirmed the decreased expression of BRCC36 (Fig. 1I). Taken together, these findings suggest that BRCC36 levels decrease during CKD-induced VC, indicating a potential role of BRCC36 in the regulation of this process.

BRCC36 alleviates vascular calcification in mice

Because of the decreased BRCC36 expression in calcified radial arteries and vessel tissues from CKD mice, we treated male C57BL/6J mice with adeno-associated virus 9 (AAV9) to overexpress or knockdown BRCC36 (Fig. S2A). As anticipated, BRCC36 was successfully overexpressed or knocked down in mouse aortas, as confirmed by western blot analysis (Fig. 2A, S2B). Following a 12-week period of high-adenine and high-phosphate diet feeding, the overexpression of BRCC36 led to a decrease in the expression of the osteogenic protein RUNX2 and an increase in the expression of the contractile protein α-SMA in mouse aortas (Fig. 2B). Additionally, Von Kossa staining and Alizarin Red S staining revealed that the aortas of AdBRCC36 group mice presented decreased levels of calcium deposition (Fig. 2C). IHC and IF staining demonstrated that RUNX2 expression was significantly downregulated in the AdBRCC36 group (Fig. 2C, D). Conversely, BRCC36 knockdown greatly exacerbated VC progression (Fig. 2E–H). The whole-mount Alizarin Red S staining results for the full-length aorta confirmed the aforementioned conclusion (Fig. 2I). Overall, these results further suggested that BRCC36 can alleviate VC in vivo.

BRCC36 regulates the osteogenic transdifferentiation of VSMCs in vitro

According to data from in vivo experiments, BRCC36 likely plays a VC-protective role. Thus, we established a BRCC36 gain-of-function VSMC model with adenovirus Ad-BRCC36 or the small interfering RNA (si-BRCC36) for immunoblotting, Alizarin Red S staining, and calcium content assays. The overexpression and knockdown efficiencies were assessed by immunoblotting (Fig. S3A, B). BRCC36 overexpression counteracted the increase in RUNX2, bone morphogenetic protein 2 (BMP2), and calcium deposition and partially reversed the decrease in α-SMA protein expression induced by CM (Fig. 3A–C). Conversely, BRCC36 silencing had the opposite effects (Fig. 3D–G). To further elucidate the role of BRCC36 in VSMC osteoblastic differentiation, VSMCs cultured in CM were treated with G5 (1 μM), a BRCC36 small molecule inhibitor. The efficacy of G5 was verified by western blot analysis (Fig. S3C). As shown in Fig. 3H–K, G5 exacerbated the calcium deposition induced by CM, and immunoblotting revealed further increases in the expression of RUNX2 and further decreases in the expression of α-SMA, indicating that the inhibitor G5 promoted VSMC osteogenic transdifferentiation. These results indicated that BRCC36 prevents the osteogenic differentiation and calcium deposition of VSMCs.

BRCC36 inhibits VC via the Wnt/β-catenin signalling pathway

The pro-calcification and pro-osteogenic effects of the Wnt/β-catenin signalling pathway have been extensively

(See figure on next page.)

Fig. 3 BRCC36 regulates the osteogenic transdifferentiation of VSMCs in vitro. **A** Western blot analysis of RUNX2, BMP2, and α-SMA expression in VSMCs. n = 3 per group. **B** Photomicrographs of Alizarin Red S staining in VSMCs pretransfected with indicated treatment. **C** Calcium content in VSMCs from all of the experimental cohorts. n = 4 per group. **D**, **E** Western blot analysis of BMP2 and α-SMA expression in VSMCs. n = 4 per group. **F** Calcium content in VSMCs from all of the experimental cohorts (n = 4 per group). **G** Photomicrographs of Alizarin Red S staining in VSMCs pretransfected with indicated treatment. **H** Western blot analysis of RUNX2 and α-SMA expression in VSMCs. n = 4 per group. **I** Calcium content in VSMCs from all of the experimental cohorts. n = 4 per group. **J** Photomicrographs of Alizarin Red S staining in VSMCs pretreated with indicated treatment. **K** Quantitative real-time PCR analysis of OCN, ALP, and SM22α expression in VSMCs, which were pretreated with G5. Statistical significance was assessed using two tailed t-test (**E**) and 1-way ANOVA followed by Dunnett's test (**A**, **C**, **F**, **H**, **I**, **K**). All values are presented as mean ± SD. *$P < 0.05$

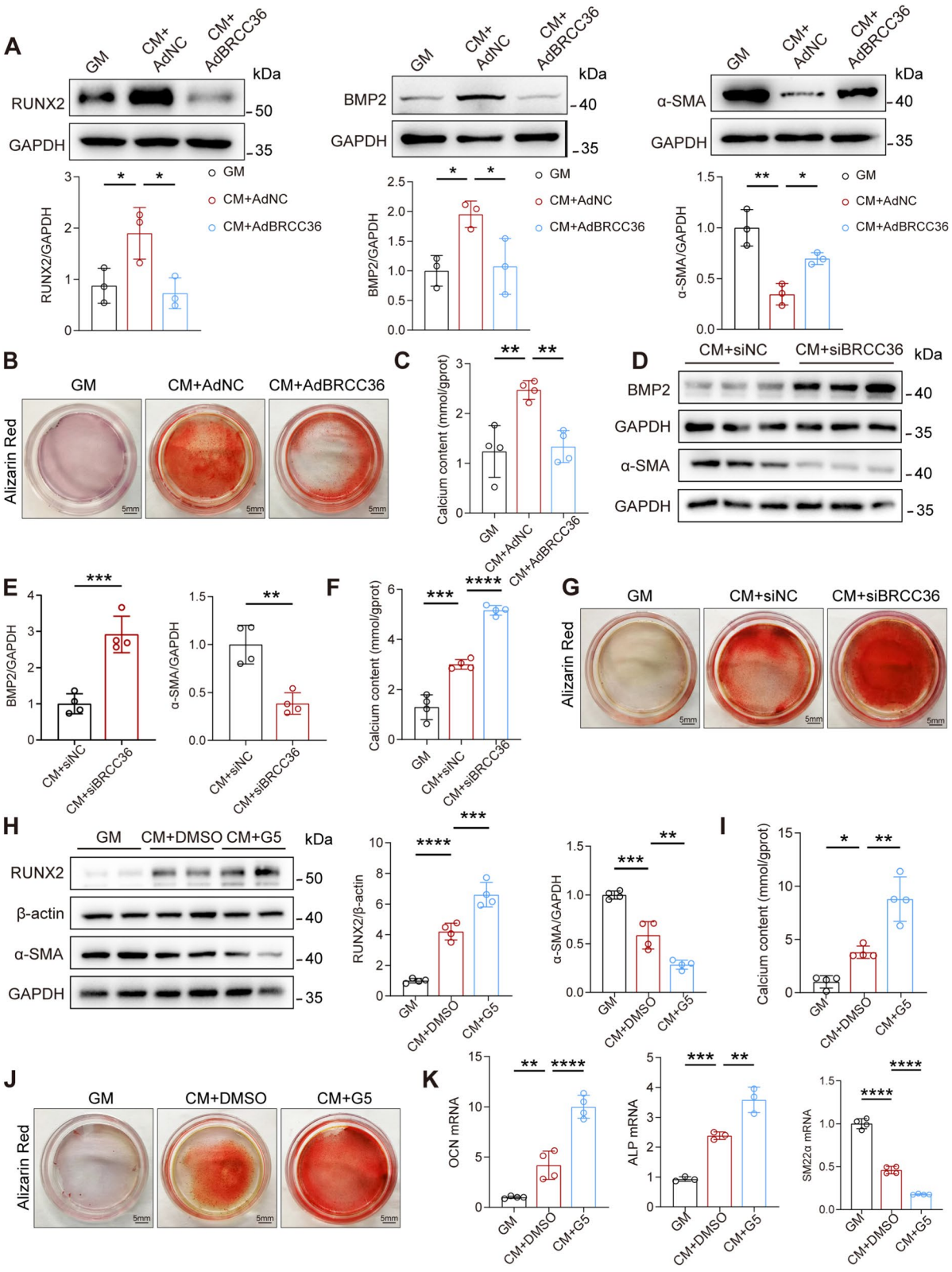

Fig. 3 (See legend on previous page.)

reported, and BRCC36 is closely associated with β-catenin in the osteogenic differentiation of osteoblasts [22, 23]. We first confirmed that β-catenin expression was significantly increased in arteries from CKD patients and that its nuclear localization was negatively correlated with BRCC36 expression (Fig. 4A, B). To test whether the Wnt/β-catenin signalling pathway mediated the effect of BRCC36 in VC, CKD mice were treated with an inhibitor of the Wnt/β-catenin signalling pathway, MSAB (Fig. S4A). Western blot analysis revealed that MSAB reversed BRCC36-knockdown-induced VSMC osteogenic transdifferentiation (Fig. 4C, D). Von Kossa staining, Alizarin Red S staining, RUNX2 IHC staining, and double immunofluorescence staining also revealed that the promoting effect of BRCC36 knockdown on calcium deposition was attenuated by MSAB (Fig. 4E–G). Furthermore, in reciprocal BRCC36 gain-of-function experiments, treatment with SKL2001 (a specific agonist of the Wnt/β-catenin signalling pathway) reversed the protective effects of BRCC36 overexpression (Fig. 4H, I). Conversely, treatment with MSAB (a β-catenin selective inhibitor) attenuated BRCC36 silencing-enhanced VC (Fig. 4J, K). These results further suggest that BRCC36 exerts protective effects at least partially via the Wnt/β-catenin signalling pathway.

BRCC36 suppresses β-catenin nuclear translocation and transcriptional activity by inhibiting K63-linked β-catenin polyubiquitination

To elucidate the molecular mechanisms by which BRCC36 regulates the Wnt/β-catenin signalling pathway, we consulted the STRING database and performed protein–protein docking analysis to test whether there was an interaction between BRCC36 and β-catenin. We obtained a docking score of -296.4 and an interaction surface area of 4264.52 between BRCC36 and β-catenin, suggesting a high likelihood of interaction between these two proteins (Fig. 5A, B). Immunofluorescence double staining further confirmed the colocalization of BRCC36 and β-catenin in VSMCs (Fig. 5C). β-catenin IP with cell lysates from VSMCs was then performed to confirm the interaction between endogenous BRCC36 and β-catenin proteins (Fig. 5D). HEK293T cells were simultaneously treated with Flag-tagged BRCC36 and His-tagged β-catenin. Co-IP analysis demonstrated that exogenously overexpressed Flag-BRCC36 could bind to His-β-catenin in HEK293T cells (Fig. 5D). To identify the BRCC36-interacting domains of β-catenin, β-catenin deletion constructs were generated (Fig. 5E). β-catenin interacted with BRCC36 mainly through its N-terminal domain (amino acids 1–664), as determined by Co-IP assays (Fig. 5F).

Previous studies have reported that BRCC36 mainly regulates the K63-dependent ubiquitination of its substrate proteins [24]. Western blot analysis demonstrated that CM obviously increased the K63-mediated polyubiquitination of β-catenin and that BRCC36 overexpression suppressed this change (Fig. 5G). Cultured VSMCs infected with Ad-BRCC36 presented decreased nuclear translocation of β-catenin (Fig. 5H). Moreover, β-catenin reporter (TOPFlash) assays revealed that BRCC36 overexpression decreased β-catenin transcriptional activity (Fig. 5I). BRCC36 overexpression reduced the phosphorylation level of β-catenin at S675, a known site that augments β-catenin transcriptional activity (Fig. 5J). Additionally, western blot and RT–PCR results demonstrated that BRCC36 overexpression downregulated the expression of the classic Wnt/β-catenin target genes c-myc and cyclin D1 at both the protein and mRNA levels (Fig. 5J, K). These results suggest that BRCC36 might inhibit the Wnt/β-catenin signalling pathway by regulating the level of K63-linked ubiquitination of β-catenin.

Pioglitazone attenuates VC partly through upregulating BRCC36 expression and downregulating β-catenin expression

Our preliminary work demonstrated that pioglitazone (PIO) inhibits VSMC calcification by inhibiting the activity of the Wnt/β-catenin signalling pathway [9]. These results demonstrated that BRCC36 also suppresses the

(See figure on next page.)

Fig. 4 BRCC36 inhibits VC via the Wnt/β-catenin signalling pathway. **A** Representative IHC staining of β-catenin in CKD patients without and with vascular calcification. Positive staining is shown in brown. Scale bar, 50 μm. n = 5 per group. **B** Correlation of BRCC36 positive staining (%) with β-catenin positive nuclei. Correlation was determined via the Pearson test (n = 10). **C**, **D** Western blot analysis of RUNX2 and α-SMA protein levels in aortic tissues. n = 6 per group. **E** Representative Von Kossa staining, Alizarin Red S staining, and IHC staining of RUNX2 images in aortas among all groups. Scale bar, 200 μm. n = 6 per group. **F** Representative IF staining of RUNX2 and α-SMA images in aortas among all groups. Scale bar, 100 μm. n = 6 per group. **G** Representative Alizarin Red S staining images of the whole aortas. Scale bar, 5 mm. **H** Western blot analysis of α-SMA protein levels in VSMCs. n = 3 per group. **I** Photomicrographs of Alizarin Red S staining in VSMCs for different pretreatments. **J** Western blot analysis of RUNX2 protein levels in VSMCs. n = 4 per group. **K** Photomicrographs of Alizarin Red S staining in VSMCs for different pretreatments. Statistical significance was assessed using two tailed t-test (**A**) and 1-way ANOVA followed by Dunnett's test (**D**, **E**, **F**, **H**, **J**). All values are presented as mean ± SD. *$P < 0.05$

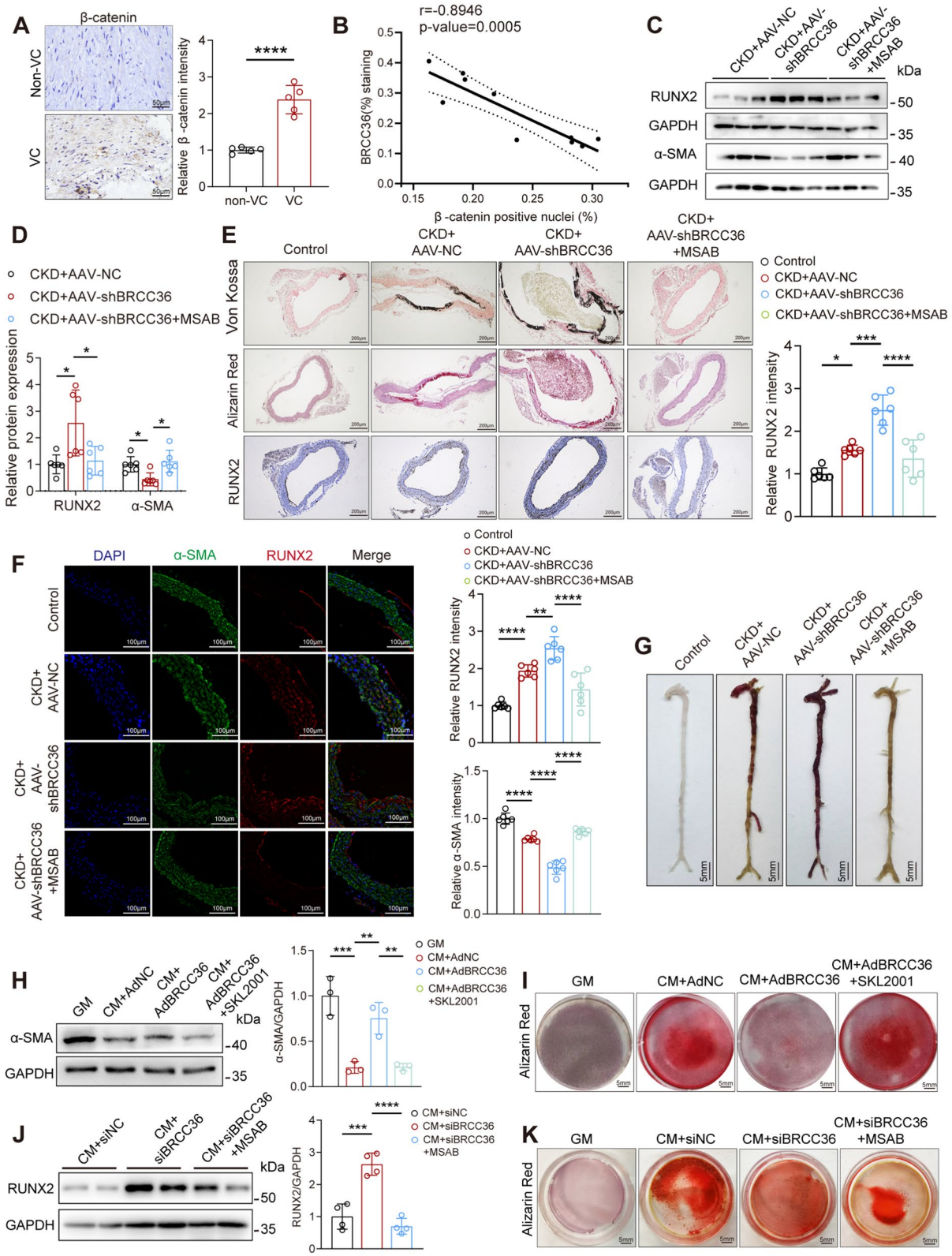

Fig. 4 (See legend on previous page.)

activity of the Wnt/β-catenin signalling pathway. We therefore surmise that PIO exerts its protective effect on VC partly by upregulating BRCC36 and thereby modulating the Wnt/β-catenin pathway. These experimental hypotheses raised by our study were first tested by in vivo studies (Fig. 6A). After 12 weeks of administration of 10 mg/kg/day PIO via oral gavage, the aortic calcium salt deposition in CKD mice was indeed attenuated, as verified by Von Kossa and Alizarin Red S staining (Fig. 6B). RUNX2 IHC and IF staining results also revealed that PIO treatment decreased the expression of the osteogenic differentiation marker RUNX2 in the aorta (Fig. 6C, D). Consistent with our hypothesis, the IHC staining results indicated that PIO significantly increased BRCC36 expression and decreased β-catenin expression in the aortas of CKD mice (Fig. 6E, F). Alizarin Red S staining revealed that PIO inhibited mineralization in VSMCs (Fig. 6G). Next, the affinity between PIO and the BRCC36 protein was analysed via molecular docking (Fig. 6H). The results showed that PIO bound to BRCC36 through visible hydrogen bonds. The Thr171 residue plays a key role in the hydrogen bond interaction between PIO and BRCC36. PIO and BRCC36 had a low binding energy of − 5.6 kcal/mol, indicating good binding activity. These results demonstrated that BRCC36 may be a key protein responsible for the anticalcification activity of PIO. Further in vitro validation via western blot analysis confirmed that PIO upregulated BRCC36 expression and downregulated β-catenin expression in VSMCs under both GM and CM culture conditions (Fig. 6I–L).

Discussion

This is the first study to examine the role of BRCC36 in experimental VC in CKD rodents and VC in CKD patients. As summarized in Fig. 7, the major findings are as follows: (1) BRCC36 expression was decreased in the radial arteries of patients with CKD, in aortic tissues from CKD animal models, and in calcified VSMCs; (2) VSMC-BRCC36-overexpressing mice were somewhat protected against VC, and VSMC-BRCC36-knockdown mice presented aggravated VC; (3) BRCC36 suppressed the Wnt/β-catenin pathway by decreasing the K63 ubiquitination level of β-catenin in VSMCs; and (4) PIO attenuated VC development partially by increasing BRCC36 expression and decreasing β-catenin expression.

VC is a highly regulated and complex process that involves multiple mechanisms, including oxidative stress, the release of calcifying matrix vesicles, inflammation, mitochondrial dysfunction, cell senescence and apoptosis, epigenetic alterations, etc. [4, 7, 25–28]. Protein ubiquitination and deubiquitination play indispensable roles in VC development by regulating the signal transduction, localization and degradation of substrate proteins [29]. Deubiquitinating enzymes (DUBs) are powerful regulators of cell fate and are highly promising drug targets in clinical practice [30]. The present study was built on our previous work to elucidate the role of BRCC36 in VC in vivo and in vitro [23]. First, our results indicated that BRCC36 expression was downregulated in calcified radial arteries and aortic tissues in vivo and in osteogenic VSMCs. Our in vivo experiments confirmed that the overexpression of BRCC36 reduced aortic calcification in CKD mice; the opposite results were obtained after BRCC36 knockdown. Our investigation also demonstrated that BRCC36 overexpression reduced the expression of osteogenic markers, as well as mineralization, in VSMCs cultured with CM. Conversely, BRCC36 silencing and inhibition exacerbated VC.

Previous studies have indicated that the osteogenic differentiation of VSMCs appears to be initiated prior to mineral deposition [31]. Although our study underscores the pivotal role of BRCC36 in the pathogenesis of VC by inhibiting the phenotypic transdifferentiation of VSMCs, there could also be additional mechanisms that remain to be explored. There is nearly a consensus that the apoptosis of VSMCs significantly increases during the VC process and that the release of apoptotic bodies from VSMCs, which act as nucleation sites for hydroxyapatite, can initiate VC [32]. Liu et al. reported that BRCC36 inhibition induced apoptosis in internal-tandem duplication

(See figure on next page.)

Fig. 5 BRCC36 suppresses β-catenin nuclear translocation and transcriptional activity by inhibiting K63-linked β-catenin polyubiquitination. **A** Predicted BRCC36-β-catenin interaction was done by STRING database. **B** Molecular docking assays of BRCC36 and β-catenin. **C** The co-localization of BRCC36 and β-catenin in VSMCs was detected by double-labeling immunofluorescence. Scale bar, 50 μm. **D** BRCC36 interaction with β-catenin in VSMCs and exogenous interaction of BRCC36 and β-catenin in HEK293T cells was detected by Co-IP. **E** A diagram showing the plasmid construct containing different domains of β-catenin. **F** The exact domain of β-catenin interacts with BRCC36 was determined by Co-IP. **G** The K63 ubiquitination alterations of β-catenin were detected by western blotting after BRCC36 overexpression. **H** Detection of β-catenin localization by nucleocytoplasmic separation experiments after BRCC36 overexpression. **I** The activity of the Wnt/β-catenin signaling pathway was detected by TOP/FOPFlash assay. **J** VSMCs were transfected with Ad-vector or Ad-BRCC36. Western blot analysis of protein levels of β-catenin S675, c-myc, cyclinD1, and β-actin. **K** RT-qPCR analysis of the mRNA levels of c-myc and cyclin D1, n = 6 per group. Statistical significance was assessed using two tailed t-test (**H**, **I**, **J**, **K**). All values are presented as mean ± SD. *$P < 0.05$

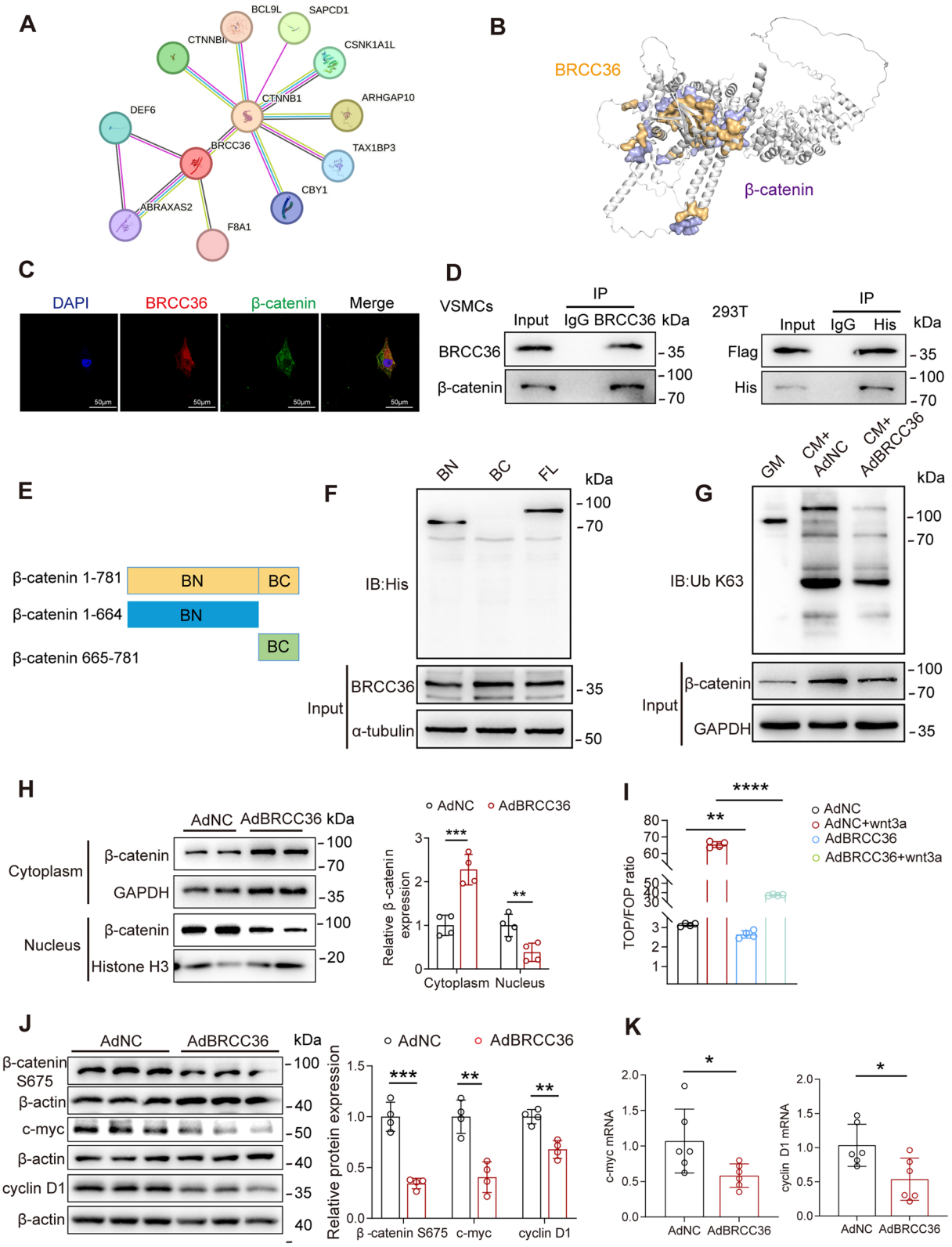

Fig. 5 (See legend on previous page.)

domain (ITD)-positive cells [33]. However, another study revealed that BRCC36 can alleviate pulmonary hypertension (PH) by inhibiting apoptosis resistance, extracellular matrix production, and phenotypic transformation in pulmonary arterial smooth muscle cells [17]. This discrepancy may be due to the different disease models used. Ferroptosis, a form of nonapoptotic cell death, is characterized by lipid peroxidation and excessive iron-dependent reactive oxygen species (ROS) [34]. A growing body of evidence indicates that ferroptosis contributes to VC by disrupting normal cellular functions. For example, Ye et al. reported that VSMC ferroptosis was triggered under CKD conditions to promote VC by suppressing the SLC7A11/GSH/GPX4 axis [35]. Furthermore, ferroptosis in VSMCs mediated by solute carrier family 39 member 14 (Slc39a14) and solute carrier family 39 member 8 (Slc39a8) promoted VC, and deferoxamine (DFO), an iron chelator, effectively alleviated VC [36]. Recent research has suggested that BRCC36 inhibits ferroptosis by stabilizing 3-hydroxy-3-methylglutaryl-coenzyme A reductase (HMGCR) in a DUB-dependent manner [37]. Therefore, BRCC36 likely exerts its protective effects through other VC-related signalling pathways. Proteomics, transcriptomics, genomics, or metabolomics-based approaches should be used to further explore the underlying regulatory mechanisms of BRCC36 in VC. The exploration of the usefulness of BRCC36 agonists in impeding VC is highly important.

Numerous studies have demonstrated that the activation of the WNT/β-catenin signalling pathway is important for VC development [12]. Previous studies have shown that BRCC36 can regulate the osteogenic differentiation of osteoblasts through β-catenin signalling [22]. Given that VC shares common regulatory mechanisms with bone formation [38], we conformed that β-catenin nuclear expression was negatively correlated with BRCC36 expression in clinical radial artery samples. In vivo experiments corroborated that the β-catenin inhibitor MSAB reversed the pro-calcification effects of BRCC36 knockdown. In vitro reversion experiments using β-catenin inhibitors and agonists in VSMCs supported our results.

Mechanistically, β-catenin may be a critical regulator of the effects of BRCC36 on the osteogenic differentiation of VSMCs. However, how does BRCC36 influence the function of β-catenin? The function and activity of the Wnt/β-catenin signalling pathway are tightly regulated by ubiquitination [39]. Previous studies have shown that unspliced XBP1 (uXBP1) weakens VC by promoting K48 polyubiquitination and subsequent degradation of β-catenin, further confirming that β-catenin ubiquitination affects VC progression [40]. To elucidate the mechanism involved, we first identified the interaction between BRCC36 and β-catenin through a STRING database search and molecular docking, colocalization (immunofluorescence double staining), and Co-IP assays. Additionally, by generating truncation constructs of β-catenin, we confirmed that β-catenin bound to BRCC36 via its N-terminal domain. K63-dependent β-catenin ubiquitination was increased under calcifying conditions, an effect that was reduced by BRCC36 overexpression. BRCC36 overexpression also reduced Wnt activity, as determined by TopFlash/FopFlash analysis, and downregulated the expression of classic β-catenin target genes (cyclin D1 and c-myc). Additionally, using nucleocytoplasmic separation experiments, we demonstrated that BRCC36 blocked the nuclear translocation of β-catenin and decreased the phosphorylation of β-catenin at S675, subsequently resulting in a reduction in the transcriptional activity of β-catenin. In summary, our study indicated that BRCC36 exerts its anticalcification effect partly through β-catenin signalling.

In the present study, our findings suggest that BRCC36 overexpression reduces the expression of cyclin D1, a marker of cell proliferation. VSMC proliferation is a critical cellular event in the pathogenesis of diverse vascular lesions and signifies an increase in collagen synthesis, further resulting in luminal narrowing and artery stiffening [41]. Sclerostin has been reported to play a potential inhibitory role in VC, accompanied by the suppression of VSMC proliferation [32]. Glucagon-like peptide-1

(See figure on next page.)

Fig. 6 Pioglitazone attenuates VC partly through upregulating BRCC36 expression. **A** Schematic overview of process for exploring the role of PIO influencing VC in vivo. **B** Representative Von Kossa staining and Alizarin Red S staining images in aortas among all groups. Scale bar, 200 μm. n = 6 per group. **C** Representative IHC staining of RUNX2 images in aortas among all groups. Scale bar: upper panels: 200 μm; lower panels: 50 μm. n = 6 per group. **D** Representative IF images of RUNX2 and α-SMA in aortas among all groups. Scale bar, 100 μm. **E** Representative IHC staining of BRCC36 images in aortas among all groups. Scale bar: upper panels: 200 μm; lower panels: 50 μm. n = 6 per group. **F** Representative IHC staining of β-catenin images in aortas among all groups. Scale bar: upper panels: 200 μm; lower panels: 50 μm. n = 6 per group. **G** Representative Alizarin Red S staining in VSMCs pretransfected with indicated treatment. **H** Molecular docking of pioglitazone and BRCC36 was performed using AutoDock and visualized using PyMOL. The yellow dashed lines indicate hydrogen bonds. **I**, **J** BRCC36 and β-catenin immunoblotting in VSMCs cultured in growth medium after PIO treatment. n = 4 per group. **K**, **L** BRCC36, β-catenin and α-SMA immunoblotting in VSMCs cultured in calcified medium after PIO treatment. n = 4 per group

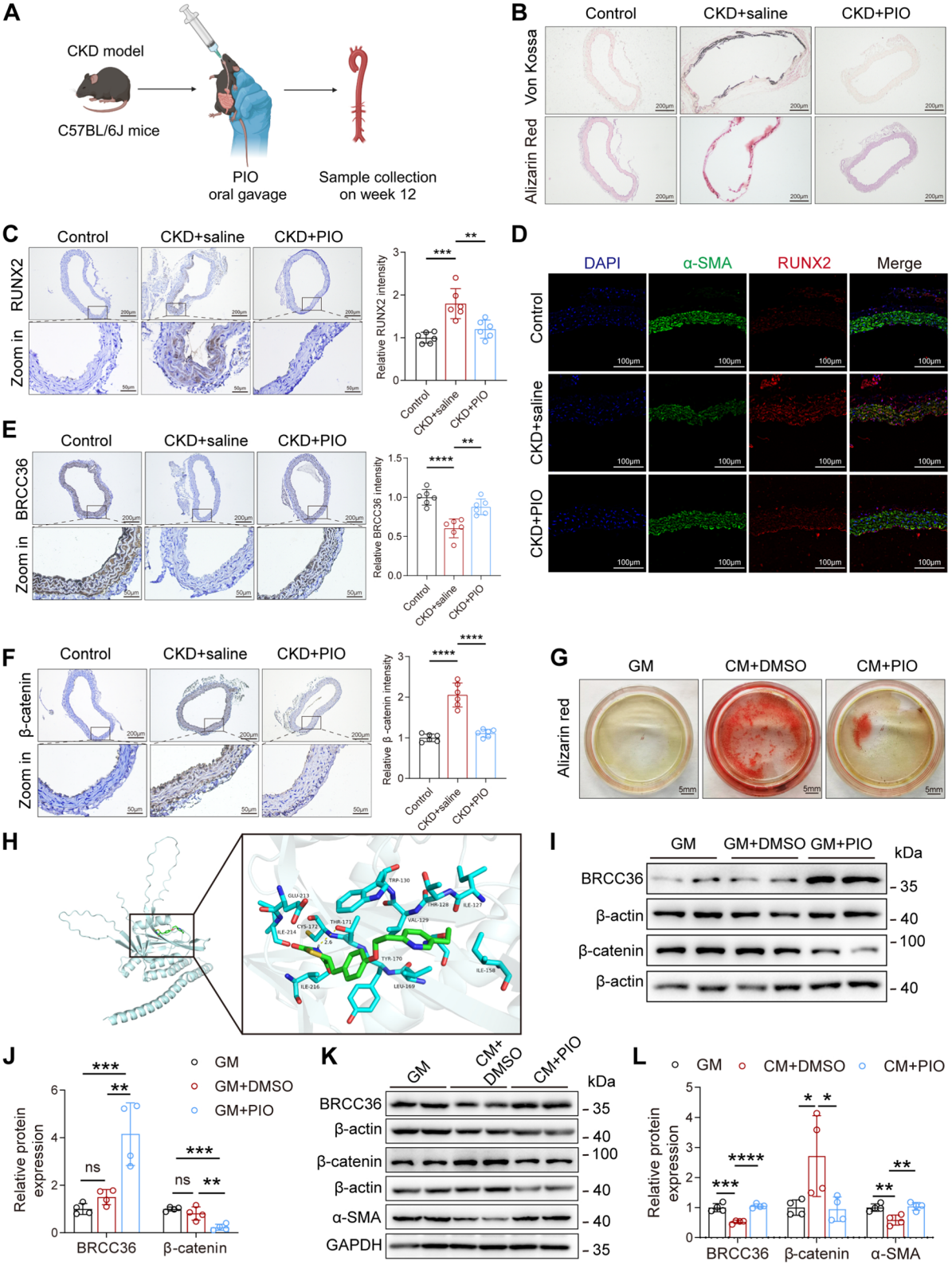

Fig. 6 (See legend on previous page.)

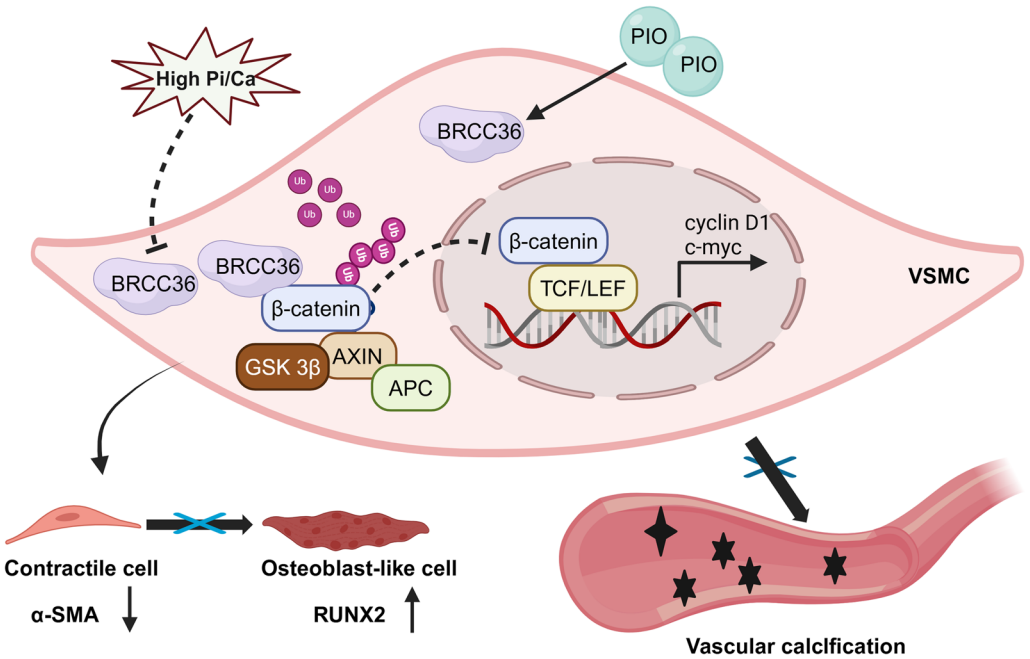

Fig. 7 The schematic of BRCC36-mediated regulation of β-catenin and VC development. BRCC36 alleviates vascular calcification by decreasing the ubiquitination of β-catenin and inhibiting its transcriptional activity. Pioglitazone attenuates VC partly by upregulating BRCC36 expression. Rectification of the BRCC36-β-catenin axis may ameliorate VC in CKD

receptor agonists (GLP-1RAs) suppress atherosclerotic progression by reducing calcium deposits, inhibiting VSMC proliferation and decreasing the expression of cyclin D1 [42]. Moreover, elevated cytosolic calcium levels in pulmonary arterial smooth muscle cells (PASMCs) are involved in cell proliferation [43]. However, whether BRCC36 affects VSMC proliferation and whether VSMC proliferation mediates the beneficial effects of BRCC36 in VC have not yet been elucidated. Further studies are needed to explore these issues.

PIO has gained widespread attention for its versatile beneficial effects on numerous cardiovascular diseases [44]. Studies have demonstrated that PIO reverses pulmonary hypertension and right heart failure by preventing lipid accumulation and restoring mitochondrial function [45].Among patients with stroke, those who were treated with PIO had a reduced absolute risk of myocardial infarction and total recurrent stroke compared with those treated with placebo [46]. Our previous study revealed that PIO alleviated VC in a VSMC model in vitro by inhibiting the Wnt/β-catenin signalling [9]. Considering the critical role of BRCC36 in β-catenin function, we next explored the effect of PIO on BRCC36 expression and found that PIO upregulated BRCC36 expression both in vivo and in vitro. Shen H et al. reported that PIO administration could ameliorate pulmonary hypertension caused by BRCC36 loss in Sugen5416/hypoxic mice [17]. Our data preliminarily revealed that PIO upregulated BRCC36 expression in the aortic tissues of CKD mice and VSMCs and further elucidated some of the mechanisms by which pioglitazone affects VC; however, our results did not further confirm that BRCC36 was a direct target of PIO via pull-down assays and proteomic microarrays. It will therefore be necessary to conduct more follow-up experiments to supplement and improve our conclusions.

Our study has the following limitations. First, we should perform in vivo experiments using VSMC-specific BRCC36-knockdown and BRCC36-knockin transgenic mice to ensure accuracy. Second, the high adenine and high phosphorus-induced CKD model is relatively limited, and another CKD mouse model should be established using the 5/6 nephrectomy technique to validate the above results. Third, we demonstrated the interaction between BRCC36 and β-catenin by endogenous and exogenous Co-IP experiments, a semiendogenous Co-IP experiment is needed to further confirm our conclusions. Fourth, although we conclude that BRCC36 alleviates VC by decreasing K63 ubiquitination of β-catenin, the precise ubiquitination sites on β-catenin targeted by BRCC36 are still unknown. Identification of the ubiquitination sites on β-catenin via mass spectrometry analysis and systematic lysine mutation is imperative. Investigating the mechanisms underlying BRCC36 dysregulation in

the development/progression of VC would also be highly interesting.

Conclusions

In summary, our study revealed an association between decreased BRCC36 expression and overactivation of the Wnt/β-catenin signalling pathway during VC progression. We found that BRCC36-mediated deubiquitination suppressed the Wnt/β-catenin signalling pathway. These findings identify BRCC36 and β-catenin as potential targets for the prevention of VC.

Abbreviations

α-SMA	Alpha-smooth muscle actin
SM22α	Smooth muscle protein 22-alpha
BMP2	Bone morphogenetic protein 2
BRCC36	BRCA1/BRCA2-containing complex subunit 3
CKD	Chronic kidney disease
CM	Calcifying media
GM	Growth media
HEK293	Human embryonic kidney 293
HMGCR	3-Hydroxy-3-methylglutaryl-coenzyme A reductase
NLRP3	Nucleotide-binding oligomerization domain-like receptor family pyrin domain-containing 3
PAS	Periodic acid-Schiff
RUNX2	Runt-related transcription factor 2
siRNA	Small interfering RNA
Slc39a14	Solute carrier family 39 member 14
Slc39a8	Solute carrier family 39 member 8
Ub	Ubiquitin
VC	Vascular calcification
VSMCs	Vascular smooth muscle cells

Supplementary Information

The online version contains supplementary material available at https://doi.org/10.1186/s12967-024-05605-w.

Additional file 1: Figure S1. The successful construction of CKD mouse model and identification of primary VSMCs. Figure S2. Animal experimental design and validation of BRCC36 knockdown efficiency. Figure S3. Verification of overexpression, knockdown and inhibitory efficiency of BRCC36. Figure S4. Schematic illustration of the animal experiment design. Table S1. The relative siRNA in this work. Table S2. The antibodies used in this study. Table S3. The primers of relative genes in this work.

Acknowledgements

Thanks to all participants involved in this research. The figures are created with www.BioRender.com.

Author contributions

YL and HM: Writing-original draft, Investigation, Formal analysis, Data curation, Conceptualization. XC and YQ: Methodology, Conceptualization. XX, CX, MM and DL: Writing-review and editing, supervision. CC and HM: Writing-review and editing, Supervision, Resources, Project administration, Funding acquisition, Conceptualization.

Funding

This work was supported by the Priority Academic Program Development (PAPD) of Jiangsu Higher Education Institutions (CN) and the National Natural Science Foundation of China (81970639, 82151320).

Availability of data and materials

All data and materials in the article can be requested from the corresponding author.

Declarations

Ethics approval and consent to participate

All human experiments were approved by the Human Research Ethics Committee of the First Affiliated Hospital of Nanjing Medical University (approval number: 2024-SR-251).
All animal experiments were approved by the Institutional Animal Ethics Committee of Nanjing Medical University (approval number: IACUC-2312015).

Consent for publication

Not applicable.

Competing interests

The authors declare that the research was conducted in the absence of any commercial or financial relationships that could be construed as a potential competing interests.

Author details

[1]Department of Nephrology, Jiangsu Province Hospital, The First Affiliated Hospital of Nanjing Medical University, Nanjing, #300 Guangzhou Road, 210029, China. [2]Department of Medical Science, Yangzhou Polytechnic College, #458 West Wenchang Road, Yangzhou 225009, China. [3]Department of General Medicine, The Second Hospital of Nanjing, Affiliated to Nanjing University of Chinese Medicine, #1-1 Zhongfu Road, Nanjing 210003, China.

Received: 8 July 2024 Accepted: 18 August 2024
Published online: 03 September 2024

References

1. Zhang H, Li G, Yu X, Yang J, Jiang A, Cheng H, et al. Progression of vascular calcification and clinical outcomes in patients receiving maintenance dialysis. JAMA Netw Open. 2023;6(5): e2310909.
2. Górriz JL, Molina P, Cerverón MJ, Vila R, Bover J, Nieto J, et al. Vascular calcification in patients with nondialysis CKD over 3 years. Clin J Am Soc Nephrol. 2015;10(4):654–66.
3. Han Y, Zhang J, Huang S, Cheng N, Zhang C, Li Y, et al. MicroRNA-223-3p inhibits vascular calcification and the osteogenic switch of vascular smooth muscle cells. J Biol Chem. 2021;296: 100483.
4. Hao QY, Yan J, Wei JT, Zeng YH, Feng LY, Que DD, et al. Prevotella copri promotes vascular calcification via lipopolysaccharide through activation of NF-κB signaling pathway. Gut Microbes. 2024;16(1):2351532.
5. Lanzer P, Hannan FM, Lanzer JD, Janzen J, Raggi P, Furniss D, et al. Medial arterial calcification: JACC state-of-the-art review. J Am Coll Cardiol. 2021;78(11):1145–65.
6. Adelnia H, Moonshi SS, Wu Y, Bulmer AC, Mckinnon R, Fastier-Wooller JW, et al. A bioactive disintegrable polymer nanoparticle for synergistic vascular anticalcification. ACS Nano. 2023;17(19):18775–91.
7. Ouyang L, Su X, Li W, Tang L, Zhang M, Zhu Y, et al. ALKBH1-demethylated DNA N6-methyladenine modification triggers vascular calcification via osteogenic reprogramming in chronic kidney disease. J Clin Invest. 2021;131(14): e146985.
8. Zhang T, Zhu M, Ma J, Liu Z, Zhang Z, Chen M, et al. Moscatilin inhibits vascular calcification by activating IL13RA2-dependent inhibition of STAT3 and attenuating the WNT3/β-catenin signalling pathway. J Adv Res. 2024. https://doi.org/10.1016/j.jare.2024.02.020.
9. Gao M, Chen T, Wu L, Zhao X, Mao H, Xing C. Effect of pioglitazone on the calcification of rat vascular smooth muscle cells through the downregulation of the Wnt/β-catenin signaling pathway. Mol Med Rep. 2017;16(5):6208–13.
10. Schunk SJ, Floege J, Fliser D, Speer T. WNT-β-catenin signalling—a versatile player in kidney injury and repair. Nat Rev Nephrol. 2021;17(3):172–84.
11. Xiong L, Guo HH, Pan JX, Ren X, Lee D, Chen L, et al. ATP6AP2, a regulator of LRP6/β-catenin protein trafficking, promotes Wnt/β-catenin signaling and bone formation in a cell type dependent manner. Bone Res. 2024;12(1):33.
12. Al-Huseini I, Ashida N, Kimura T. Deletion of IκB-kinase β in smooth muscle cells induces vascular calcification through β-catenin-runt-related transcription factor 2 signaling. J Am Heart Assoc. 2018;7(1): e007405.

13. Wang C, Huang M, Lin Y, Zhang Y, Pan J, Jiang C, et al. ENO2-derived phosphoenolpyruvate functions as an endogenous inhibitor of HDAC1 and confers resistance to antiangiogenic therapy. Nat Metab. 2023;5(10):1765–86.
14. Thibeault S, Rautureau Y, Oubaha M, Faubert D, Wilkes BC, Delisle C, et al. S-nitrosylation of beta-catenin by eNOS-derived NO promotes VEGF-induced endothelial cell permeability. Mol Cell. 2010;39(3):468–76.
15. Na J, Shaji S, Hanemann CO. Targeting histone deacetylase 6 (HDAC6) to enhance radiation therapy in meningiomas in a 2D and 3D in vitro study. EBioMedicine. 2024;105: 105211.
16. Chen Z, Lin B, Yao X, Weng J, Liu J, He Q, et al. Endothelial β-catenin upregulation and Y142 phosphorylation drive diabetic angiogenesis via upregulating KDR/HDAC9. Cell Commun Signal. 2024;22(1):182.
17. Shen H, Gao Y, Ge D, Tan M, Yin Q, Wei TW, et al. BRCC3 regulation of ALK2 in vascular smooth muscle cells: implication in pulmonary hypertension. Circulation. 2024;150(2):132–50.
18. Dong Y, Hakimi MA, Chen X, Kumaraswamy E, Cooch NS, Godwin AK, et al. Regulation of BRCC, a holoenzyme complex containing BRCA1 and BRCA2, by a signalosome-like subunit and its role in DNA repair. Mol Cell. 2003;12(5):1087–99.
19. Liu D, Jin S, Cui J. The TRIM14-USP14-BRCC36 complex epigenetically regulates inflammation through inhibiting OPTN-mediated autophagic degradation of KDM4D. Autophagy. 2022;18(8):2001–2.
20. Yalcinkaya M, Liu W, Thomas LA, Olszewska M, Xiao T, Abramowicz S, et al. BRCC3-mediated NLRP3 deubiquitylation promotes inflammasome activation and atherosclerosis in Tet2 clonal hematopoiesis. Circulation. 2023;148(22):1764–77.
21. Walden M, Tian L, Ross RL, Sykora UM, Byrne DP, Hesketh EL, et al. Metabolic control of BRISC-SHMT2 assembly regulates immune signalling. Nature. 2019;570(7760):194–9.
22. Cai L, Huo Z, Yang H, He F, Cao Z, Wu F, et al. Gene co-expression network analysis identifies BRCC3 as a key regulator in osteogenic differentiation of osteoblasts through a β-catenin signaling dependent pathway. Iran J Basic Med Sci. 2019;22(2):173–8.
23. Xie C, Chen C, Wu L, Xiong Y, Xing C, Mao H. BRCC36 prevents vascular calcification in chronic kidney disease through the β-catenin signalling pathway. Exp Cell Res. 2022;413(1): 113051.
24. Kim JS, Kim HK, Lee J, Jang S, Cho E, Mun SJ, et al. Inhibition of CD82 improves colitis by increasing NLRP3 deubiquitination by BRCC3. Cell Mol Immunol. 2023;20(2):189–200.
25. Ballester-Servera C, Alonso J, Cañes L, Vázquez-Sufuentes P, García-Redondo AB, Rodríguez C, et al. Lysyl oxidase in ectopic cardiovascular calcification: role of oxidative stress. Antioxidants (Basel). 2024;13(5):523.
26. Wang ZX, Luo ZW, Li FX, Cao J, Rao SS, Liu YW, et al. Aged bone matrix-derived extracellular vesicles as a messenger for calcification paradox. Nat Commun. 2022;13(1):1453.
27. Villa-Bellosta R. Dietary magnesium supplementation improves lifespan in a mouse model of progeria. EMBO Mol Med. 2020;12(10): e12423.
28. Cui L, Zhou Q, Zheng X, Sun B, Zhao S. Mitoquinone attenuates vascular calcification by suppressing oxidative stress and reducing apoptosis of vascular smooth muscle cells via the Keap1/Nrf2 pathway. Free Radic Biol Med. 2020;161:23–31.
29. Xu P, Liu Y, Liu C, Guey B, Li L, Melenec P, et al. The CRL5-SPSB3 ubiquitin ligase targets nuclear cGAS for degradation. Nature. 2024;627(8005):873–9.
30. Gao H, Xi Z, Dai J, Xue J, Guan X, Zhao L, et al. Drug resistance mechanisms and treatment strategies mediated by Ubiquitin-Specific Proteases (USPs) in cancers: new directions and therapeutic options. Mol Cancer. 2024;23(1):88.
31. Zhang K, Zhang Y, Feng W, Chen R, Chen J, Touyz RM, et al. Interleukin-18 enhances vascular calcification and osteogenic differentiation of vascular smooth muscle cells through TRPM7 activation. Arterioscler Thromb Vasc Biol. 2017;37(10):1933–43.
32. González-Salvatierra S, García-Fontana C, Lacal J, Andújar-Vera F, Martínez-Heredia L, Sanabria-de la Torre R, et al. Cardioprotective function of sclerostin by reducing calcium deposition, proliferation, and apoptosis in human vascular smooth muscle cells. Cardiovasc Diabetol. 2023;22(1):301.
33. Liu J, Isaji T, Komatsu S, Sun Y, Xu X, Fukuda T, et al. BRCC36 associates with FLT3-ITD to regulate its protein stability and intracellular signaling in acute myeloid leukemia. Cancer Sci. 2024;115(4):1196–208.
34. Wang Y, Gan X, Cheng X, Jia Y, Wang G, Tang X, et al. ABCC2 induces metabolic vulnerability and cellular ferroptosis via enhanced glutathione efflux in gastric cancer. Clin Transl Med. 2024;14(8): e1754.
35. Ye Y, Chen A, Li L, Liang Q, Wang S, Dong Q, et al. Repression of the antiporter SLC7A11/glutathione/glutathione peroxidase 4 axis drives ferroptosis of vascular smooth muscle cells to facilitate vascular calcification. Kidney Int. 2022;102(6):1259–75.
36. Aierken Y, He H, Li R, Lin Z, Xu T, Zhang L, et al. Inhibition of Slc39a14/Slc39a8 reduce vascular calcification via alleviating iron overload induced ferroptosis in vascular smooth muscle cells. Cardiovasc Diabetol. 2024;23(1):186.
37. Wang H, Shu L, Lv C, Liu N, Long Y, Peng X, et al. BRCC36 deubiquitinates HMGCR to regulate the interplay between ferroptosis and pyroptosis. Adv Sci (Weinh). 2024;11(11): e2304263.
38. Chen J, Ren T, Xie L, Hu H, Li X, Maitusong M, et al. Enhancing aortic valve drug delivery with PAR2-targeting magnetic nano-cargoes for calcification alleviation. Nat Commun. 2024;15(1):557.
39. Lin Y, Chen X, Lin L, Xu B, Zhu X, Lin X. Sesamolin serves as an MYH14 inhibitor to sensitize endometrial cancer to chemotherapy and endocrine therapy via suppressing MYH9/GSK3β/β-catenin signaling. Cell Mol Biol Lett. 2024;29(1):63.
40. Yang L, Dai R, Wu H, Cai Z, Xie N, Zhang X, et al. Unspliced XBP1 counteracts β-catenin to inhibit vascular calcification. Circ Res. 2022;130(2):213–29.
41. Ma Q, Yang Q, Xu J, Zhang X, Kim D, Liu Z, et al. ATIC-associated de novo purine synthesis is critically involved in proliferative arterial disease. Circulation. 2022;146(19):1444–60.
42. Lee J, Hong SW, Kim MJ, Moon SJ, Kwon H, Park SE, et al. Glucagon-like peptide receptor agonist inhibits angiotensin II-induced proliferation and migration in vascular smooth muscle cells and ameliorates phosphate-induced vascular smooth muscle cells calcification. Diabetes Metab J. 2024;48(1):83–96.
43. Chen J, Rodriguez M, Miao J, Liao J, Jain PP, Zhao M, et al. Mechanosensitive channel Piezo1 is required for pulmonary artery smooth muscle cell proliferation. Am J Physiol Lung Cell Mol Physiol. 2022;322(5):L737–60.
44. Lee SH, Kim N, Kim M, Woo SH, Han I, Park J, et al. Single-cell transcriptomics reveal cellular diversity of aortic valve and the immunomodulation by PPARγ during hyperlipidemia. Nat Commun. 2022;13(1):5461.
45. Legchenko E, Chouvarine P, Borchert P, et al. PPARγ agonist pioglitazone reverses pulmonary hypertension and prevents right heart failure via fatty acid oxidation. Sci Transl Med. 2018;10(438):eaao0303.
46. Dawson J. Pioglitazone use after stroke: story of hearts, minds, and bones. Circulation. 2018;138(12):1221–3.

Publisher's Note